Applied Catalysis B: Environmental 249 (2019) 42–53

Contents lists available at ScienceDirect

Applied Catalysis B: Environmental

journal homepage: www.elsevier.com/locate/apcatb

Engineering of activated carbon surface to enhance the catalytic activity of supported cobalt oxide nanoparticles in peroxymonosulfate activation

Juan C. Espinosa[a], Premkumar Manickam-Periyaraman[a], Francisco Bernat-Quesada[a], Subramanian Sivanesan[b], Mercedes Álvaro[a], Hermenegildo García[a,c,*], Sergio Navalón[a,*]

[a] Departamento de Química and Instituto de Tecnología Química CSIC-UPV, Universitat Politècnica de València, Consejo Superior de Investigaciones Científicas, Av. de los Naranjos s/n, 46022, Valencia, Spain
[b] Department of Applied Science and Technology, Anna University, Sardar Patel Road, 600025, Chennai, India
[c] Center of Excellence for Advanced Materials Research, King Abdulaziz University, Jeddah, Saudi Arabia

ARTICLE INFO

Keywords:
Heterogeneous catalysis
Activation mechanism
Peroxymonosulfate reagent
Cobalt oxide nanoparticles
Functionalized activated carbon

ABSTRACT

Commercial activated carbon has been functionalized by chemical or thermal treatments to introduce surface oxygen functional groups able to anchor small cobalt nanoparticles with superior catalytic activity for peroxymonosulfate activation. The resulting activated carbon supports where characterized by combustion elemental analysis, Fourier-transformed infrared spectroscopy, Raman spectroscopy, isothermal N_2 adsorption, temperature programmed desorption/mass spectrometry, X-ray diffraction and scanning electron microscopy. Activated carbon functionalization by nitric acid resulted the most appropriated method to provide a higher population of oxygenated functional groups able to anchor small cobalt nanoparticles. The catalytic activity of supported oxidized metal nanoparticles (4.7 ± 0.05 nm) was higher than analogous non-oxidized cobalt nanoparticles (2.9 ± 0.14 nm). The use of analogous supported oxidized iron or copper nanoparticles resulted in lower catalytic activity. Importantly, the supported oxidized cobalt nanoparticles at 0.2 wt% loading exhibit higher activity than benchmark catalysts such as unsupported Co_3O_4 solid or even homogeneous Co^{2+} ions. This is a reflection of the relatively low estimated activation energy for both processes, peroxymonosulfate decomposition and phenol degradation. The estimated activation energy values are about 30 and 32 kJ mol^{-1}. The stability of the most active catalyst was assessed by performing eight consecutive uses without observing decrease of catalytic activity, neither metal leaching or metal nanoparticle aggregation. Turnover numbers/turnover frequencies values as high as $4{\cdot}10^5/8{\cdot}10^5$ h^{-1} for peroxymonosulfate activation and $39{\cdot}10^3/68{\cdot}10^3$ h^{-1} for phenol degradation at pH 7 and 20 °C have been estimated, respectively. Electron paramagnetic resonance measurements and selective quenching experiments revealed that the generated sulfate radicals from peroxymonosulfate rapidly are transformed in highly reactive hydroxyl radicals. In excellent agreement with previous reports, this work demonstrates the importance of an adequate activated carbon functionalization to obtain superior and stable catalysts for peroxymonosulfate activation.

1. Introduction

Advanced oxidation processes (AOPs) are a class of chemical treatments for pollutant remediation in soil [1,2], water [3–5] and air [6]. The aim of AOPs is the generation of highly aggressive radicals such as HO$^{\cdot}$, HOO$^{\cdot}$ or $SO_4^{\cdot -}$ that able to attack virtually any organic contaminant in aqueous media triggering their aerobic degradation and, eventually, their mineralization [5,7]. In the field of waste water treatments AOPs are frequently employed to degrade recalcitrant, toxic and/or non-biodegradable compounds that cannot be treated using conventional biological water treatments [8]. One of the AOPs with easiest implementation is the (photo)Fenton reaction that employs Fe (II) salts and H_2O_2 at acidic pH (~3) to generate hydroxyl radicals from H_2O_2 [3,5]. One of the main drawbacks, however, of the (photo)Fenton reaction is the need of acidic pH values in order to avoid iron precipitation. The use of acidic pH values is also beneficial for H_2O_2 stability since at basic pH values it decomposes spuriously to O_2 without generating HO$^{\cdot}$ radicals. An alternative AOP treatment that is less pH dependent based on the Co(II) ions as homogeneous catalyst to activate peroxymonosulfate (PMS) to generate sulfate radicals ($SO_4^{\cdot -}$) [9–11].

* Corresponding authors at: Departamento de Química and Instituto de Tecnología Química CSIC-UPV, Universitat Politècnica de València, Consejo Superior de Investigaciones Científicas, Av. de los Naranjos s/n, 46022, Valencia, Spain.
E-mail addresses: hgarcia@qim.upv.es (H. García), sernaol@doctor.upv.es (S. Navalón).

https://doi.org/10.1016/j.apcatb.2019.02.043
Received 23 October 2018; Received in revised form 29 January 2019; Accepted 8 February 2019
Available online 21 February 2019
0926-3373/ © 2019 Elsevier B.V. All rights reserved.

It is worth to mention that in comparison to Fe(II), Co(II) ions remain soluble in aqueous solutions at pH values below 9.4 [9,10]. Importantly, PMS can operate efficiently at higher pH values including neutral aqueous solutions [9]. At basic pH values PMS decomposition occurs spontaneously at high rates without the need of any catalyst, the challenge being at room temperature developing catalyst for pH values below 7 [11,12]. Sulfate radicals have an oxidation potential fairly independent on the pH value of about 2.5–3.1 V vs standard hydrogen electrode, while, in contrast, the redox potential of hydroxyl radicals is strongly dependent of the pH ranging from 1.8 to 2.7 [10]. In addition, sulfate radicals have a longer half-life (30–40 μs) compared to hydroxyl radicals (1 μs) [10].

Regardless the good pollutant degradation efficiencies achieved using the commented homogeneous AOPs under optimal reaction conditions, practical applications are limited due to the need of removal from the treated waters of dissolved transition metals employed in the process to avoid negative environmental impacts and risks for the human health [4,5,10,11]. Cobalt concentration is typically limited in drinking water to values lower than 50 $\mu g\,L^{-1}$ [11]. The removal of the transition metal ions is generally carried out by precipitation with the disadvantage of needing further addition of chemicals and the subsequent sludge formation. Furthermore, in order to accomplish the water quality regulations, the removal of these transition metal ions should be done at levels below micrograms per liter [13]. These reasons, strongly limit the practical applications of homogenous AOPs using transition metals other than Fe.

In order to solve these problems, heterogeneous catalytic AOPs have been developed [10,11,14–16]. Frequently, metal or metal oxide NPs are supported on a high surface area insoluble material, allowing the easy recovery and immobilization of the transition metal [10,11,14,15]. In this context, cobalt species are among the most catalyst for PMS activation, leading to the generation of oxyl radicals [17–24]. Recently, nanocarbon materials have also been employed as heterogeneous carbocatalysts for PMS activation [25,26].

However, in spite of the advances done in the field of heterogeneous cobalt-based catalysts for PMS activation, there still remain some challenges to increase further the activity and stability of the catalysts. Among these challenges, those dealing with the preparation of small metal NPs and their stabilization through a strong interaction with the support are crucial to obtain highly efficient and stable materials [10,11,27].

The present work shows the importance of an adequate surface functionalization of activated carbon to support small, active and stable cobalt oxide NPs able to activate PMS at neutral or acidic pH values. In this way, efficient heterogeneous catalyst promoting phenol degradation at neutral and acidic pH values as aqueous model pollutant has been obtained. The highest activity has been determined for the catalyst having the smallest cobalt oxide NPs. Thus, it will be shown that commercial active carbon functionalized by HNO_3 acid treatment under optimal conditions is a suitable support to deposit small cobalt oxide NPs with enhanced catalytic activity. In contrast, activated carbon functionalization with a controlled thermal oxidation results in a catalyst with lower activity due to the bigger cobalt oxide NPs are formed. The influence of the cobalt oxidation state on the resulting catalytic activity has been also evaluated, observing that cobalt oxide NPs are more active than reduced cobalt. Importantly, the activated carbon supported cobalt oxide catalyst can be reused at least eight times at neutral pH and room temperature without observing neither loss of catalytic activity nor metal leaching. Selective quenching experiments and electron paramagnetic resonance (EPR) spectroscopic study prove that PMS activation using the supported cobalt oxide catalyst generates hydroxyl radicals.

2. Experimental section

2.1. Materials

Oxone® (potassium peroxymonosulfate, PMS) ($KHSO_5{\cdot}1/2KHSO_4{\cdot}1/2K_2SO_4$, MW 307.38), commercial activated carbon (AC, Norit SX Ultra, ref. 53663), $Co(NO_3)_2{\cdot}6H_2O$ (> 99.999% purity), Co_3O_4 nanopowder (< 50 nm particle size based on transmission electron microscopy measurements) and phenol (> 99.5% purity based on gas chromatography analysis) were supplied by Sigma-Aldrich (Madrid, Spain). Other reactants or solvents employed were analytical or high performance liquid chromatography (HPLC) grade and they were also supplied by Sigma-Aldrich (Madrid, Spain).

2.2. Methods

2.2.1. Commercial activated carbon functionalization by nitric acid

Briefly, commercial AC (1 g) was dispersed in concentrated nitric acid (65%, 25 mL) in a round-bottom flask (100 mL) and the system heated at 83 °C for 24 h. Once the system was cooled down to room temperature, the suspension was transferred to two centrifuge tubes (20 mL each) and, then, the suspension centrifuged at 14,000 rpm for 20 min. Then, the supernatant liquid was disposed in an appropriate acid liquid residue container. Subsequently, the centrifuge tubes containing the solid sample were filled with Milli-Q water (20 mL each) and dispersed using a laboratory Vortex mixer. Several consecutive centrifugation-redispersion washings with Milli-Q water were performed until the pH of the supernatant was neutral. Finally, the solid was dried in an oven at 100 °C for 24 h and the sample labelled as ACN.

2.2.2. AC functionalization by thermal treatment

Briefly, commercial AC (200 mg) placed in a ceramic crucible was heated (7 $°C\,min^{-1}$) in an oven under static air up to 420 °C and, this temperature was maintained for 2 h. Then, the sample was cooled down to room temperature and labelled as ACT.

2.2.3. Deposition of cobalt NPs on the AC supports (Co/ACs)

Cobalt NPs were supported on commercial AC, ACN and ACT solids by using the polyol method [28]. Briefly, the corresponding active carbon support (200 mg) placed in a round-bottomed flask (250 mL) was suspended with ethylene glycol (80 mL). Activated carbon was dispersed in ethylene glycol by sonication for 20 min. Subsequently, the flask was placed in a heat-on block and magnetically stirred. Then, the appropriate amount of cobalt salt dissolved in water (1 mL) was added to the suspension to achieve the required metal loading (0.2 or 1 wt%) and the system was heated at 85 °C for 4 h under magnetic stirring. After cooling the system at room temperature, ethanol (80 mL) was added to the flask containing the solid catalyst in ethylene glycol to favor solid sedimentation during centrifugation. Then, the mixture was transferred to eight centrifuge tubes (20 mL each) and centrifuged at 14,000 rpm for 20 min. At this time, the supernatant was removed, additional ethanol (20 mL per centrifuge tube) was added and the sediment redispersed using a Vortex mixer. This process was repeated four times using Milli-Q water as solvent. Finally, the sediment in each centrifuge tube was suspended again using Milli-Q water (20 mL) and the dispersion placed in a round-bottomed flask (250 mL). The flask was frozen using liquid nitrogen and, then, freeze-dried using a lyophilizer (Telstar LyoQuest). The resulting samples were labelled as Co/AC, Co/ACN or Co/ACT. These solid samples (200 mg) were further oxidized in an oven under static air at 180 °C for 2 h and the samples labelled as Co_{ox}/AC, Co_{ox}/ACN or Co_{ox}/ACT. Analogous Fe_{ox} or Cu_{ox} supported on ACN catalysts were also prepared using this methodology employing $Fe(NO_3){\cdot}7H_2O$ or $Cu(NO_3)_2$ salts as metal precursors.

Unsupported cobalt oxide NPs were prepared by reduction of an aqueous solution (25 mL) containing cobalt nitrate hexahydrate (10 $mg\,mL^{-1}$) using 10-fold excess of $NaBH_4$ as reducing agent.

Although the primary particle size could be smaller, the solid agglomerate into larger particles that can be recovered by filtration (0.2 μm Nylon filter) and washed with distillated water (500 mL). Finally, the solid was placed in an oven and heated at 180 °C for 2 h.

2.3. Catalyst and activated carbon characterization

Powder X-ray diffractograms (PXRD) were collected by using a Philips X-Pert diffractometer equipped with a graphite monochromator operating at 40 kV and 45 mA that employed Ni-filtered CuKa radiation. FTIR spectra were measured by using a Bruker Tensor 27 FT-ATR instrument. Prior to recording the FTIR spectra the samples were dried in an oven for 24 h at 80 °C, then, equilibrated at room temperature before the measurements. A Perkin Elmer CHNOS analyzer was employed for combustion elemental analysis. Temperature-programmed desorption (TPD) coupled to a mass-spectrometer (TPD-MS) analyses of the active carbons (100 mg) were carried out in a Micrometer II 2920 connected to a quadrupolar mass-spectrometer measurements were carried out by heating the sample from room temperature to 900 °C at 10 °C min^{-1}. X-ray photoelectron spectroscopy (XPS) measurements were performed on a SPECS spectrometer with an MCD-9 detector using a monochromatic Al (Kα = 1486.6 eV) X-ray source. CASA software has been employed for spectra deconvolution setting at 284.4 eV [29] the C1s peak as reference. Isothermal N_2 adsorption measurements were carried out using a ASAP 2010 Micrometrics apparatus. The metal loading (Co, Fe or Cu) on the ACs was determined by inductively coupled plasma combined with optical atomic emission spectroscopy detection (ICP-OES). Cobalt leaching was assessed by ICP-OES in the liquid reaction phase after removal the solid catalyst at the end of the reaction. A JEOL JEM-2100F instrument operating at 200 kW under dark-field scanning transmission electron microscopy (DF-STEM) was employed for metal particle size estimation measuring the dimensions of more than 200 particles. Microanalysis of the particles was performed by using an EDX detector (Oxford instrument) coupled to the DF-STEM measurements.

2.4. Catalytic activity and reaction analysis

Catalytic experiments were carried out at least in duplicate. Briefly, the required amount of catalyst was added to a round-bottomed flask (500 mL) containing an aqueous phenol solution (100 mL; 100 mg L^{-1}; 1.06 mM). In order to achieve a good catalyst dispersion in the aqueous reaction medium and the system was sonicated (450 W) for 20 min analogously to previous reports [30]. The initial pH of the suspension was adjusted to the required value using aqueous solutions of NaOH (0.1 M) except for pH values below 6 were H_2SO_4 (0.1 M) was employed. If necessary the flask was placed in a heat-on block and heated at the required temperature. The corresponding amount of PMS dissolved in water (1 mL) at the corresponding pH value was added. During the course of the reaction the pH frequently was adjusted at the required value by addition of H_2SO_4 (0.1 M) or NaOH (0.1 M). During the course of the reaction several aliquots (2 mL) were taken and immediately filtered (Nylon filter 0.2 μm). Then, to each filtered reaction aliquot ten microliters of dimethylsulfoxide (DMSO) were added to quench the oxidation reaction.

In order to study the reusability of the catalyst, the catalytic reaction was carried out as commented above but using a round-bottomed flask of 1 L containing the aqueous phenol solution (600 mL; 100 mg L^{-1}; 1.06 mM). It should be commented that the use of this reaction volume allows to perform the sampling for both PMS and phenol analysis (about 2 mL each reaction aliquot) as well as recover the catalyst for at least eight consecutive reaction cycles. Thus, after each catalytic cycle the solid was recovered at the end of the reaction by filtration using a nylon membrane (0.2 μm), washed with a NaOH aqueous solution (pH 10) and then Milli-Q water to remove possible adsorbed organic or inorganic substances. It should be noted that previous studies on phenol degradation have confirmed that basic washings remove completely all the organic matter from phenol degradation [31]. Then, the catalyst was employed in a new catalytic cycle.

Productivity tests were carried out using large amount of phenol (10 g L^{-1}; 106.4 mM) and PMS (280 g L^{-1}; 911 mM) with respect to the catalyst (200 mg L^{-1}; 0.0067 mM of supported cobalt) at pH 7 and 20 °C. The catalyst was reused under these concentrations several times as previously described.

Analysis of phenol, catechol, hydroquinone and *p*-benzoquinone. Previously filtered reaction aliquots (Nylon filter 0.2 μm) were analyzed by reverse-phase liquid chromatography. The injected volume of the sample was 200 μL. A Kromasil-C18 column was employed as stationary phase. Elution was carried out under isocratic conditions (69:30:1 vol% $H_2O/CH_3CN/CH_3COOH$). The system used a photodiode array as detector. The samples from the productivity test were diluted 100-fold in Milli-Q water before analysis. The wavelengths for the detection of phenol, hydroquinone, catechol and *p*-benzoquinone were 209, 221, 230 and 245 nm, respectively.

Total organic carbon (TOC) analysis. A High-TOC Elementar II analyzer was employed for TOC measurements of previously filtered aqueous reaction aliquots. The method is based on the complete combustion of the organic matter present in the aqueous sample at 950 °C catalyzed by Pt and quantification of evolved CO_2 gas by quantitative IR spectroscopy.

PMS measurements. PMS concentration was measured using a spectrophotometric method [32]. Briefly, a previously filtered reaction aliquot (0.5 mL) was diluted with Milli-Q water (100 mL). Then, 5 mL of the diluted reaction aliquot was mixed with a KI solution (0.5 mL, 2 mg/mL) and allowed to react for 10 min before measuring its absorbance at 360 nm.

EPR measurements. EPR spectra were recorded using phenyl *tert*-butil nitrone (PBN) as spin trapping agent under the following reaction conditions: catalyst (200 mg L^{-1}, 0.0067 mM of supported cobalt), PBN (1,000 mg L^{-1}), PMS to PBN molar ratio 1, pH 7, reaction time (5 min). Previously filtered (0.2 μm) and nitrogen-purged aliquots were measured in a Bruker EMX spectrometer using the following typical settings: frequency 9.803 GHz, sweep width 3489.9 G, time constant 40.95 ms, modulation frequency 100 kHz, modulation width 1 G, and microwave power 19.92 mW.

Radical quenching experiments. Selective radical quenching experiments were carried out under the following conditions. Firstly, the catalyst (200 mg L^{-1}; 0.0067 mM) was added to a round-bottomed flask (500 mL) containing an aqueous phenol solution (100 mL, 100 mg L^{-1}). Then, the pH of the reaction system was adjusted to 7 using a NaOH aqueous solution (0.1 M). Then, the quencher agent namely DMSO (0.647 mL), methanol (0.4 mL) or *tert*-butanol (0.94 mL) was added to the phenol solution (100 mL) achieving a concentration of about 1 M. After that, the system was sonicated for 20 min. Then, the system was placed in a heating plate and magnetically stirred. Finally, PMS (280 mg dissolved in 1 mL and adjusted at pH 7) was added to the flask. The radical quencher to PMS molar ratio is about 10.

3. Results and discussion

3.1. Support preparation and characterization

The use of carbonaceous materials as metal NP supports is one of the main areas of research in heterogeneous catalysis [15]. In this sense, some examples have shown that the chemical composition, the textural properties and the groups on the surface of the carbonaceous materials determine the resulting metal particle size distribution and, therefore, the catalytic activity [27]. With these precedents in mind, our work starts with the functionalization of commercial activated carbon (Norit), referred as AC, by chemical [33,34] or thermal oxidative treatment [30]. The chemical functionalization of the activated carbon consists in a liquid phase oxidation of AC by nitric acid resulting in a sample labeled as ACN. The thermal functionalization method consists

Table 1
Textural properties and elemental analysis of the active carbons employed as catalyst support.

	C (%)	C/H molar ratio (%)	C/O molar ratio (%)	BET surface area ($m^2 g^{-1}$)	Pore volumen ($cm^3 g^{-1}$)
AC	76.7	14.3	4.5	880	0.32
ACN	58.3	5.4	2.0	710	0.26
ACT	74.3	14.9	4.0	1040	0.35

in submitting AC to an aerobic oxidation in static air at 420 °C in an oven. The thermogravimetric analysis of commercial AC solid (Fig. S1a) shows that the sample starts to undergo combustion at about 500 °C. Since the purpose of the thermal treatment is the functionalization of the commercial AC with oxygen functional groups a lower temperature was chosen in accordance to analogous previous reports [30]. The presence of oxygen in the treatment is expected to cause the partial oxidation of the most external layers of AC resulting the generation of hydroxyl, carbonyl and carboxyl functional groups. This partial oxidation will be easily confirmed by chemical analysis (Table 1) and the mineralization degree of the thermal functionalized AC sample was less than 3 wt%. In accordance with this treatment, Raman spectra do not show a decrease in the defect density. This sample is labelled as ACT. The three samples (AC, ACT and ACN) were characterized by combustion elemental analysis, FT-IR and Raman spectroscopy, isothermal N_2 adsorption, XPS, TPD-MS, XRD and SEM.

Elemental analysis data show that the oxidative treatment of AC using HNO_3 is more effective to increase the oxygen content of the carbon than that based on the thermal treatment (Table 1). In particular, the chemical treatment using HNO_3 affords a high decrease of carbon content together with a concomitant increase in oxygen content compared to ACT sample. A small increase of elemental nitrogen in the ACN sample (1.0 wt%) respect to the commercial AC sample (0.3 wt%) was also observed and attributed to the functionalization with nitrogen oxide species [33,34]. Isothermal N_2 adsorption (Figs. S1–S3) of the ACs reveals that, regardless the observed variations respect to AC, the resulting carbonaceous samples exhibits surface areas and pore volumes higher than 700 $m^2 g^{-1}$ and 0.26 $cm^3 g^{-1}$, respectively. The lower values observed for the ACN sample can be attributed to space required to accommodate a large density of oxygenated functional groups within the pores of the solid.

Raman spectroscopy of the three AC samples shows the characteristic vibrations modes due to the stretching of sp^2 carbons at 1597 cm^{-1} (G band), occurrence of disordered structure at 1317 cm^{-1} (D band) and the stacking of the sp^2 network layers at 2567 cm^{-1} (2D band) (Fig. 1a) [35]. Functionalization of AC sample by thermal or chemical methods results in an increase of the defect population as revealed by the increase in the intensity of D respect to G band [35]. FT-IR spectroscopy of the functionalized activated carbons shows an intensity increase of the peaks appearing at 1725 cm^{-1} and 1160 cm^{-1} attributable C=O and C−O stretching bands, respectively, as well as the band appearing at 1560 cm^{-1} corresponding to the presence of conjugated unsaturated C=C bonds (Fig. 1b) [34,36]. All these observations are in agreement with the increase of oxygen content observed by elemental analysis.

The three ACs were further analyzed by TPD (Fig. 2a) and TPD-MS (Fig. 2b and c) measurements under inert atmosphere. In particular, the TPD-MS allows identification by mass spectrometry of H_2O (m/z 18), CO (m/z 28) and CO_2 (m/z 44) [34]. AC functionalization by HNO_3 resulted in the introduction of a large variety of oxygen functional groups including carboxylic acids, lactones, anhydrides, phenolic, carbonyls, ether and quinone among other possible [34,36]. In the case of AC functionalization by an oxidative thermal treatment at 420 °C the resulting ACT solid results mainly functionalized with phenol, carbonyl and quinone moieties, probably because most of carboxylic acid moieties are unstable at the temperatures of the thermal treatment (420 °C) or they are not formed [34,36].

The surface of the carbonaceous materials was evaluated by XPS analyses (Figs. 3 and S5) [34]. As expected, AC oxidation by chemical or thermal treatments resulted in a shift of the C1s signals at higher binding energies indicating the oxidation of the carbon surface. In the case of O1s, an increase of the signal intensity for ACN sample or a shift to higher binding energies in the case of ACT agree with a different level of oxidation of AC sample, depending on the treatment. These observations agree with the generation of different oxygen functional groups. The oxidation of the AC by chemical or thermal treatment as well as the increase of acidic oxygen functional groups was verified by measuring the pH of aqueous suspensions of AC, ACT and ACN (10 mg mL^{-1}) corresponding to the values of 6.5, 4.8 and 3.6, respectively.

PXRD of the ACs samples reveals that the structure is maintained after the functionalization of the commercial AC. The diffractograms show the two main characteristic broad bands of activated carbons appearing at around 2θ 23 and 43° associated with the diffraction from the 002 and 100/101 planes in graphite, respectively (Fig. S4) [37]. SEM images show that the morphological structure is somehow preserved, but as the functionalization degree increases (ACN > ACT) the roughness of the AC surface increases (Fig. S6).

3.2. Metal supported on ACs

Deposition of cobalt NPs on the three activated carbons (AC, ACT and ACN) was carried out using the well-known polyol method [28,38]. In order to study the influence of the cobalt oxidation state on the catalytic activity for PMS activation, the Co NP supported on AC samples were further submitted to an aerobic oxidation under static air at 180 °C for 2 h. Several works have shown the influence of the cobalt oxidation state on PMS activation [10,11]. Table 2 summarizes the list of catalysts employed in the present work, including metal loading, average particle size distribution, standard deviation obtained from TEM measurements (Figs. 4, S7–S9) and the initial reaction rates for PMS activation and phenol degradation.

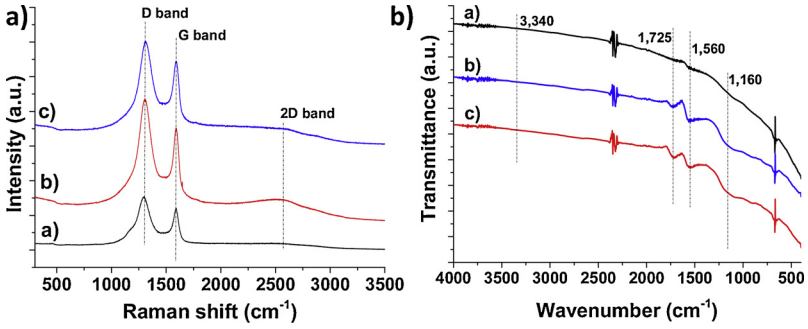

Fig. 1. Raman (a) and FT-IR (b) spectra of AC (a), ACT (b) and ACN (c) materials.

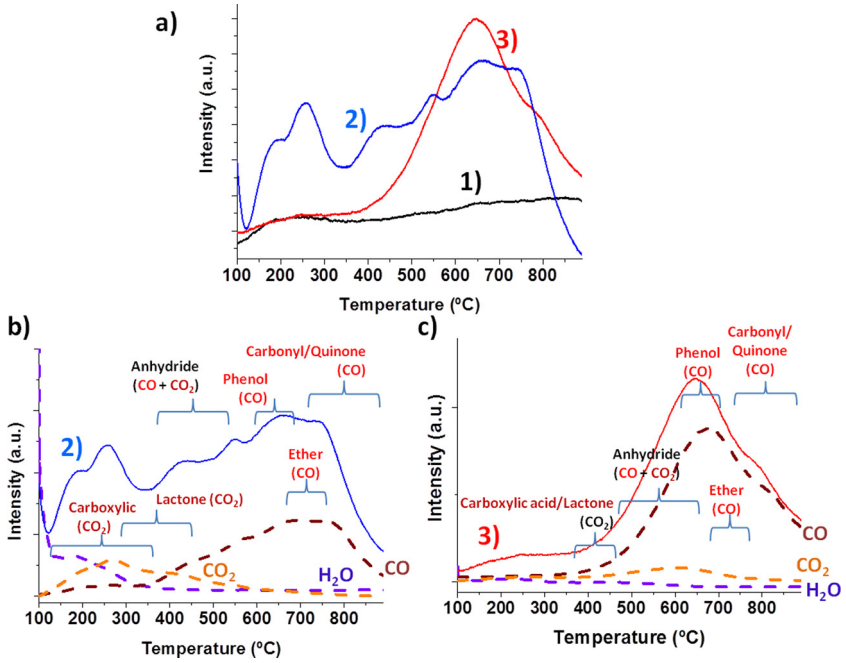

Fig. 2. TPD (a) and TPD-MS (b, c) of commercial AC (1, black line), ACN (2, blue line) and ACT (3, red line). Legend: H_2O (violet dash line), CO_2 (orange dash line) and CO (brown dash line). (For interpretation of the references to colour in this figure legend, the reader is referred to the web version of this article.)

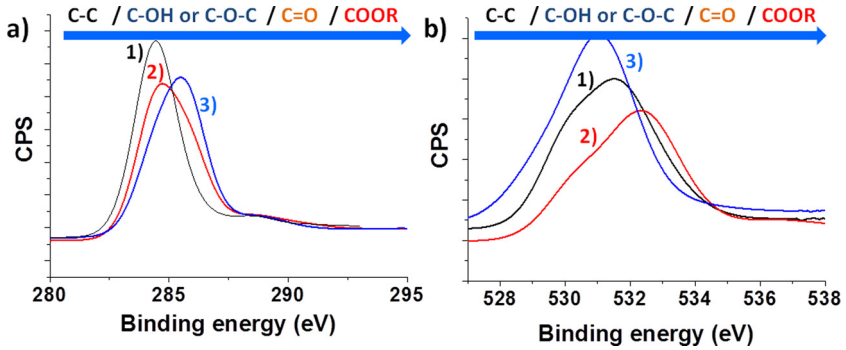

Fig. 3. XPS C1s (a) and O1s (b) peaks of AC (1, black line), ACT (2, red line) and ACN (3, blue line) (For interpretation of the references to colour in this figure legend, the reader is referred to the web version of this article.).

Table 2
Summary of the analytical and activity data for the catalysts prepared in the present work indicating metal loading, metal average particle size distribution and initial reaction rate for PMS decomposition (r0_PMS) and phenol degradation (r0_phenol).

Entry	Catalyst	Metal loading (wt%)	Average metal particle size and standard deviation (nm)	r_0_PMS ($mM\,h^{-1}$)	r_0_phenol ($mM\,h^{-1}$)
1	Co/ACN	0.2	2.9 ± 0.14	16.07	2.44
2	Co/ACT	0.2	3.3 ± 0.17	10.55	3.38
3	Co/AC	0.2	4.1 ± 0.23	8.91	3.94
4	Co_{ox}/ACN	0.2	4.7 ± 0.05	23.84	4.52
5	Co_{ox}/ACT	0.2	7.9 ± 0.26	21.22	5.25
6	Co_{ox}/AC	0.2	9.1 ± 0.25	12.51	6.40
7	Co_{ox}/ACN	1.0	5.8 ± 0.24	9.12	1.66
8	Fe_{ox}/ACN	1.0	5.6 ± 0.17	3.91	0.55
9	Cu_{ox}/ACN	1.0	6.3 ± 0.25	2.93	0.47

Selected DF-STEM images and metal particle size distribution histograms are shown in Fig. 4. Regardless the oxidation state of cobalt NPs, the smallest average cobalt particle size and standard deviation at the same metal loading is obtained using ACN as support (Table 2). Thus, it can be speculated that the presence of a high population of oxygen functional groups in ACN support is beneficial to support small metal NPs. As expected, the aerobic oxidation of cobalt NPs supported on ACs (Fig. S7) resulted in an increase of the cobalt oxide average particle size of about 2–3 nm (Table 2 and Fig. S8). Using ACN as support it was observed that an increase of the cobalt oxide content from 0.2 to 1.0 wt % resulted in an increase of both particle size distribution and standard deviation (entries 4 and 7 in Table 2 and Fig. S9). Analogous catalysts based on iron and copper oxides supported on ACN were also prepared (entries 8 and 9 in Table 2 and Fig. S9) to compare their catalytic activity with that of cobalt-based materials. Formation of cobalt NPs was confirmed by EDX analyses of different points (Fig. S10a), areas (Fig. S10b) and mapping analyses (Fig. 4). In contrast to the small cobalt oxide NPs obtained on the different carbonaceous materials, large particles (> 200 nm) were obtained when the preparation of cobalt oxide was performed without the use of any support (Fig. S11).

XPS analysis was employed to get some insights about the cobalt oxidation state of the prepared catalysts. As it will be shown below Co_{ox}/ACN is the most active catalyst for PMS activation. Initially, XPS of the Co(0.2 wt%)/ACN exposed the ambient at room temperature is composed by Co NPs whose external layers are mostly constituted by Co

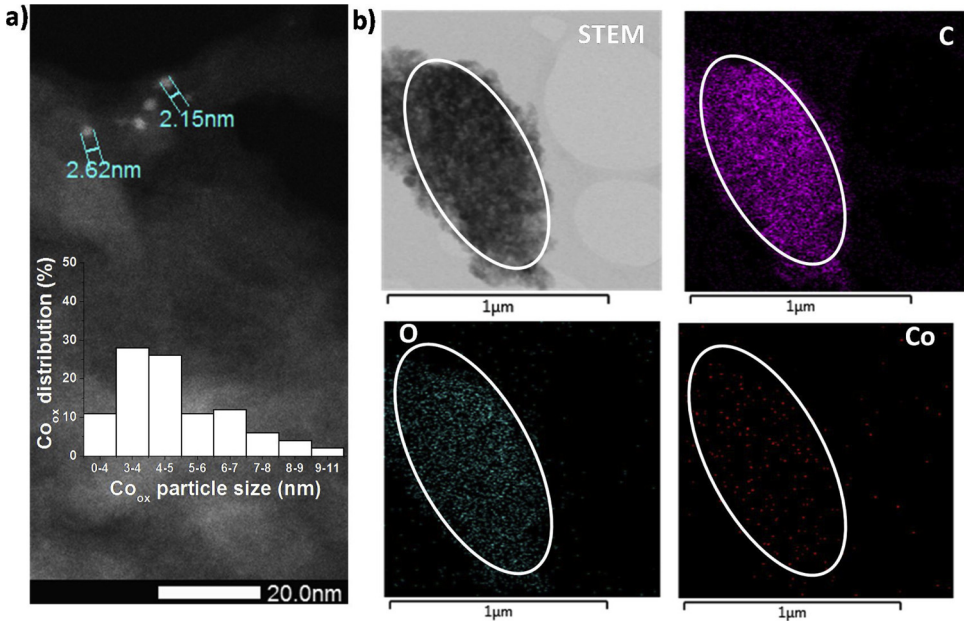

Fig. 4. a) DF-STEM image and cobalt particle distribution of Co_{ox}(0.2 wt%)/ACN; b) STEM image and element mapping microanalyses of Co_{ox}(0.2 wt%)/ACN. The inset in panel a shows the particle size distribution of cobalt oxide in Co_{ox}(0.2 wt%)/ACN.

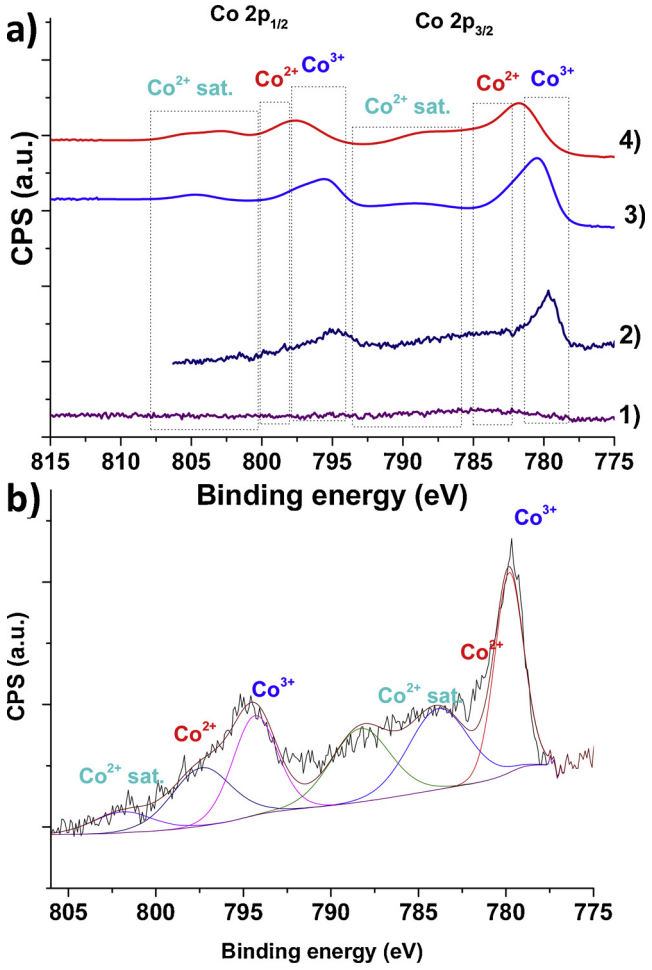

Fig. 5. XP spectra of Co(0.2 wt%)/ACN (a1), Co_{ox}(0.2 wt%)/ACN (a2), commercial Co_3O_4 solid (a3) and as-made Co_{ox} solid (5a4). Deconvoluted XP spectrum of Co_{ox}(0.2 wt%)/ACN (b).

(II) (Fig. 5a1). As expected the thermal aerobic oxidation at 180 °C for 2 h of the Co(0.2 wt%)/ACN (Fig. 5a1) solid favors the further oxidation of the most external layers of Co NPs in the Co_{ox}(0.2 wt%)/ACN solid that after the treatment are mostly constituted by Co(II) and Co(III) species (Fig. 5a2). These oxidized Co(II / III) species are similar to those observed in the case of commercial Co_3O_4 solid (Fig. 5a3) and as-made Co_{ox} solid (Fig. 5a4). For the Co_{ox}(0.2 wt%)/ACN sample, Fig. 5b shows the deconvoluted peaks at around 779.7 and 781.4 eV attributable to the Co^{3+} $2p_{3/2}$ and Co^{2+} $2p_{3/2}$, respectively. The accompanying $2p_{1/2}$ spin-orbit component for Co^{3+} and Co^{2+} appear at 794.8 and 796.8 eV, respectively. The energy difference between Co $2p_{3/2}$ and Co $2p_{1/2}$ peaks is approximately 15 eV. Two Co^{2+} satellite peaks at 786.3 and 804.8 eV are also observed. Similar deconvolution in various cobalt species is obtained for the commercial Co_3O_4 or as-made Co_{ox} solids (Fig. S12). These XPS results agree with the presence of cobalt NPs in the form of Co_3O_4 and/or CoO [39–42]. Similarly, the XPS spectra of Fe_{ox}/ACN and Cu_{ox}/ACN samples reveal the presence of oxidized metal species in the form of Fe^{3+}/Fe^{2+} or Cu^{2+}, respectively (Fig. S13) [43,44].

Diffuse reflectance UV–vis spectra of several of the cobalt oxide catalysts under study are presented in Fig. S14. Commercial Co_3O_4 and as-prepared Co_{ox} solids exhibit visible absorption bands in the regions about 400 and 650 nm that should correspond to the O^{2-}-Co^{2+} and O^{2-}-Co^{3+} ligand to metal charge transfer, respectively. In the cobalt oxide NPs supported on ACN, these absorption bands seem to be masked by the black ACN support [45].

3.3. Catalytic activity

The series of prepared catalysts was tested for phenol degradation using PMS as oxidant. Phenol was selected as organic pollutant because is a non-biodegradable, recalcitrant and toxic organic compound for the aquatic environment. Preliminary tests indicate that phenol adsorption on the three different ACs is lower than 5% (data not shown). Blank control experiments reveal that activation of PMS in the absence of catalyst is negligible at pH values below 6, but PMS decomposes faster as the pH value increases beyond pH 7 (Fig. S15), As expected, deposition of cobalt NPs supported on the carbonaceous materials increases the catalytic activity for PMS activation and phenol decomposition at pH values below 7 (Fig. 6 and Table 2). Fig. 6b shows that

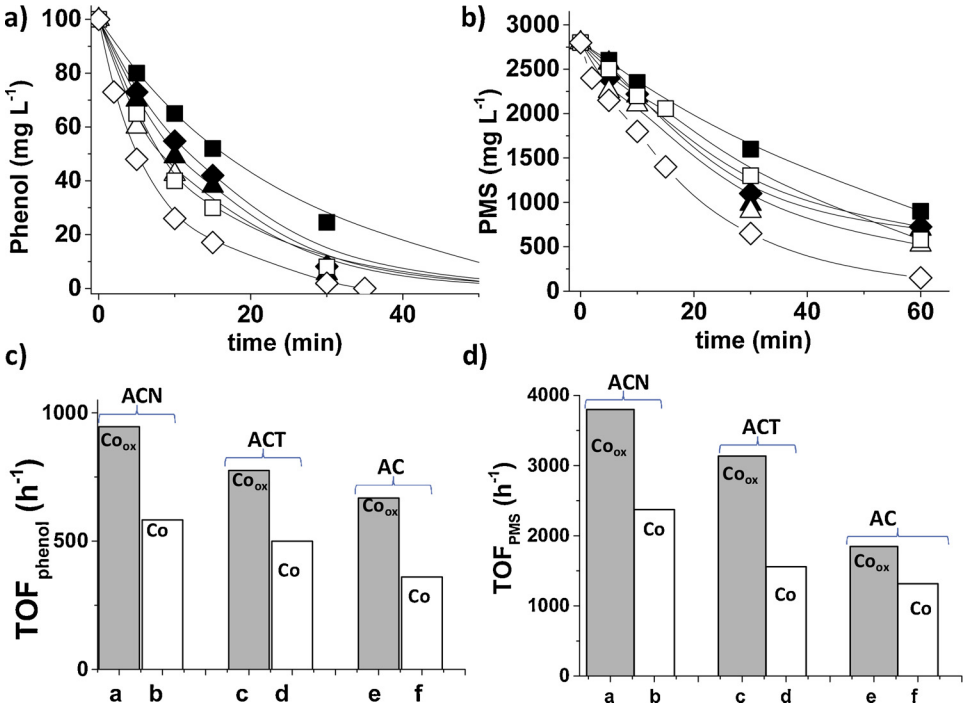

Fig. 6. Phenol degradation (a), PMS decomposition (b) and corresponding turnover frequency (TOF) value (c, d) using Co-NPs supported on AC (■, f), ACT (▲, d) and ACN (♦, b) and Co_3O_4 – NPs supported on AC (□, e), ACT (Δ, c) and ACN (◊, a). Reaction conditions: Catalyst (200 mg L^{-1}; 0.0067 mM of supported cobalt), phenol (100 mg/L; 1.06 mM), PMS (2800 mg L^{-1}; 9.1 mM), 20 °C, pH 7.

oxidized cobalt NPs supported on ACs (Co_{ox} supported on AC, ACT or ACN) are more active than analogous non-oxidized ones, even though the cobalt particle size distribution of the former indicates the larger average dimensions of Co particles after oxidation. It is a general observation in the field of catalysis by metal NPs that the catalytic activity increases as the size of the metal NP decreases [46]. In the present case, however, it seems that the oxidation state of cobalt NPs is more important than the particle size distribution for the activation of PMS. These results agree with previous reports showing the higher activity of cobalt oxides respect to metallic cobalt [10,11].

Among the different catalysts based on Co_{ox} NPs supported on ACs (AC, ACN and ACT), the highest catalytic activity has been achieved using the Co_{ox}(0.2 wt%)/ACN material that corresponds to that with the smallest cobalt oxidized metal NPs (Fig. 6). Based on the catalytic results and the characterization data of the ACs, it is proposed that the higher amount of oxygen functional groups in the ACN support generated by the chemical treatment allows a good dispersion of small cobalt NPs with enhanced catalytic activity respect to analogous ACT or AC supports. Therefore, considering the minor contribution of ACN (Fig. S15) to the catalytic activity that is mainly due to cobalt species and the relationship between small particle size and high catalytic activity (Table 2), it is proposed that the main role of the carbon support is just to stabilize cobalt NPs avoiding their growth.

Fig. 7 shows that the catalytic activity of Co_{ox} supported on ACN increases as the cobalt loading decreases from 1.0 to 0.2 wt%. This fact was attributed to the lower cobalt particle size distribution observed with the sample at lower cobalt loading. Fig. 7 also presents the influence of the metal nature on the resulting catalytic activity for phenol degradation and PMS decomposition. The catalyst based on Co_{ox} NPs supported on ACN exhibiting higher activity than analogous catalysts based on Fe_{ox} or Cu_{ox} NPs supported on ACN at the same metal loading (1 wt%).

In order to put into context the catalytic activity of Co_{ox}(0.2 wt %)ACN its catalytic activity was compared to that obtained when using homogeneous Co^{2+} ions, unsupported as-made Co_{ox} NPs or commercial Co_3O_4 solid as catalysts (Fig. 8). Frequently, phenol oxidation in water by PMS is faster when using Co^{2+} ions as homogeneous catalyst respect to the use of heterogeneous cobalt catalysts, such as cobalt oxide doped carbon aerogel [21]. Surprisingly, in the present work the activity of Co_{ox}(0.2 wt%)ACN is higher (TOF_{PMS} 3800, TOF_{phenol} 950) than that obtained using Co^{2+} ions (TOF_{PMS} 1460, TOF_{phenol} 330) or as-prepared unsupported Co_{ox} NPs (TOF_{PMS} 740, TOF_{phenol} 190). These observations highlight the importance of high surface area, AC surface functionalization with the appropriate nature and population of oxygen functional groups for the dispersion of small metal NPs with specific metal oxidation state.

One of the main problems associated with AOPs for water treatment is the strong dependence of their efficiency with the pH [14,27]. The use PMS has been reported as one promising alternative to the use of other oxidants such as H_2O_2 that typically requires strongly acidic pH solutions to achieve good efficiencies [10,11]. Herein it has been shown that Co_{ox}/ACN is an optimal catalyst for PMS activation and phenol

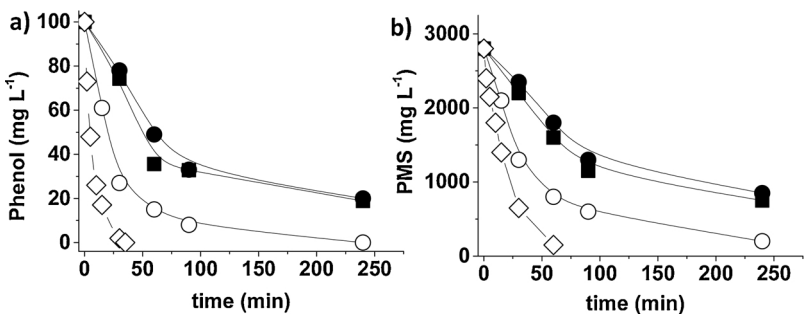

Fig. 7. Phenol degradation (a) and PMS decomposition (b) using Co_{ox}-NPs supported on ACN at 0.2 (◊) and 1 wt% cobalt loading (○). Fe_{ox}-NPs (■) and Cu_{ox}-NPs (●) supported on ACN at 1 wt% metal loading. Reaction conditions: Catalyst (0.0067 mM of supported metal), phenol (100 mg/L; 1.06 mM), PMS (2800 mg L^{-1}; 9.1 mM), 20 °C, pH 7.

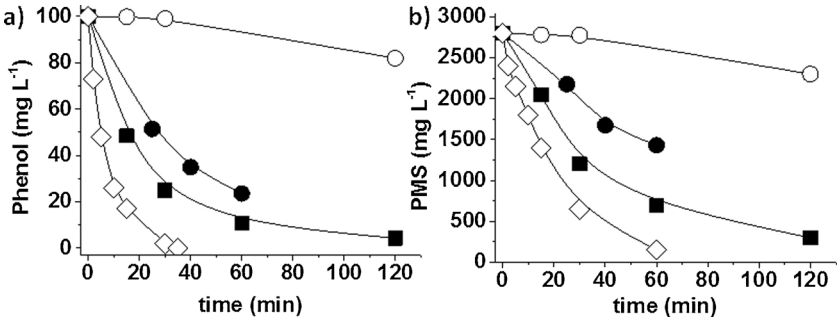

Fig. 8. Phenol degradation (a) and PMS decomposition (b) using Co_{ox} -NPs supported on ACN at 0.2 wt% metal loading (◊), using commercial Co_3O_4 NPs (○), as-prepared unsupported Co_{ox} NPs (●) and using Co^{2+} as homogeneous catalyst (■). Reaction conditions: Catalyst (0.0067 mM of cobalt either using homogeneous or heterogeneous catalysts), phenol (100 mg/L; 1.06 mM), PMS (2800 mg L^{-1}; 9.1 mM), 20 °C, pH 7.

degradation even at neutral pH values (Fig. 9). It should be reminded that PMS decomposition occurs spontaneously at an increasing rate as the pH value increases higher than 7 (Fig. S15a,b). This constitutes a significant advantage compared to other heterogeneous Fenton processes that only operate efficiently at strongly acidic pH values [3,5,14]. Previous studies using homogenous Co^{2+} ions or heterogeneous cobalt NPs supported on carbonaceous materials [47] have also found that those catalysts exhibit optimal performance at neutral or quasi-neutral pH values [10,48]. As it can be seen in Fig. 9 the catalytic activity of Co_{ox}(0.2 wt%)/ACN for PMS activation and phenol degradation increases with the pH. On one hand, an increase of the pH favors the formation of the more easily oxidizable phenolate. On the other hand, PMS decomposition should be a function of its speciation in the reaction medium [12]. Acidic pH values would increase the PMS stability and, therefore, it could make more difficult its activation towards radical formation [47,49]. Considering that PMS has a pK_2 in water about 9.4, the prevalent species at quasi-neutral pH values should be HSO_5^- (Fig. 9, Eq. (6)) and, therefore, it seems that the selective formation of $SO_4^{\bullet-}$ and/or $HO^{\bullet}$ radicals is favored (Eqs. (1), (3) and (4) [12]. Eq. (7) represents a nucleophilic attack on the peroxide hydrogen of HSO_5^- by SO_5^{2-} leading to the formation of HSO_6^- (Eq. (7)). Finally, according Eq. (8) HSO_6^- in the presence of hydroxyl ions decomposes to form O_2 through a non-radical reaction pathway. The influence of pH on the activity of the Co_{ox}(0.2 wt%)/ACN catalyst agrees with the reported prior literature data reflected by Eqs. (1)–(8).

$$Co^{2+} + HSO_5^- \rightarrow Co^{3+} + SO_4^{\bullet-} + HO^- \quad (1)$$

$$Co^{3+} + HSO_5^- \rightarrow Co^{2+} + SO_5^{\bullet-} + H^+ \quad (2)$$

$$SO_4^{\bullet-} + H_2O \rightarrow SO_4^{2-} + OH^{\bullet} + H^+ \quad (3)$$

$$SO_4^{\bullet-} + HO^- \rightarrow SO_4^{2-} + OH^{\bullet} \quad (4)$$

$$HSO_5^- + 2H_2O \rightarrow 2HO^{\bullet} + SO_4^{2-} + H^+ \quad (5)$$

$$HSO_5^- + H_2O \rightarrow SO_5^{2-} + H_3O^+ \quad (6)$$

$$HSO_5^- + SO_5^{2-} \rightarrow HSO_6^- + SO_4^{2-} \quad (7)$$

$$HSO_6^- + HO^- \rightarrow H_2O + SO_4^{2-} + O_2 \quad (8)$$

Other important parameter that should be considered when developing alternative AOPs is the amount of oxidant employed respect to the substrate [14,15,46]. Fig. 10 shows the influence of the initial PMS concentration on the catalytic activity for phenol degradation. An optimal PMS to phenol molar ratio of 9.3 was found for phenol degradation and, more importantly, degradation of its even more toxic reaction intermediates namely catechol, hydroquinone and *p*-benzoquinone (Fig. S16). This value is lower than that required in other systems for complete degradation of phenol such as cobalt oxide supported on AC (oxone to phenol molar ratio 25) [20], cobalt oxide doped on carbon aerogel [21] or carbon xerogel [50] with an oxone to phenol molar ratio 12.8 even though still some toxic intermediates such as hydroquinone and *p*-benzoquinone were detected [21]. Thus, Co_3O_4 NPs supported in reduced graphene oxide employs a phenol to PMS molar ratio of about 60 or $MnO_2/ZnFe_2O_4$ uses a phenol to PMS ratio of 31 [51]. In the present work, under optimized reaction conditions a notable TOC reduction of about 70% was measured. Furthermore, a good relationship was also observed between the TOF for phenol degradation and the amount of PMS (Fig. 10d). The TOF values increase along the PMS concentration with the maximum values of 3300 and 550 h^{-1} achieved for PMS decomposition and phenol degradation, respectively.

The catalytic activity of the most active catalyst prepared in this work Co_{ox}(0.2 wt%)/ACN using PMS as oxidant was compared with that of H_2O_2 at pH 4 and 7 (Fig. S17). The degradation of phenol by

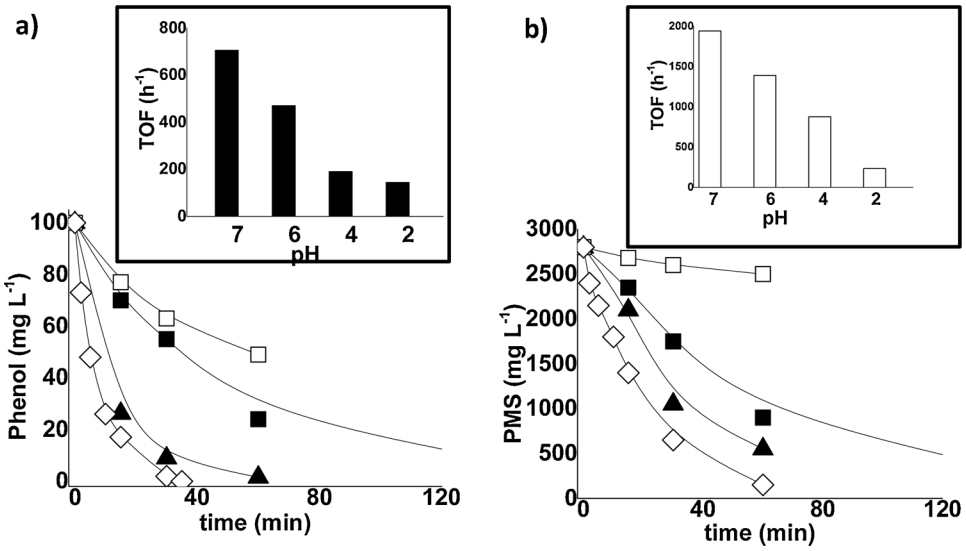

Fig. 9. Phenol degradation (a), PMS decomposition (b) and respective TOF values for phenol (black bar) and PMS (white bar) using Co_{ox} /ACN at pH 2 (□), pH4 (■), pH 6 (▲) and pH 7 (◊). Reaction conditions: Catalyst (200 mg L^{-1}; 0.0067 mM of supported cobalt), phenol (100 mg/L; 1.06 mM), PMS (2800 mg L^{-1}; 9.1 mM), 20 °C, pH as indicated.

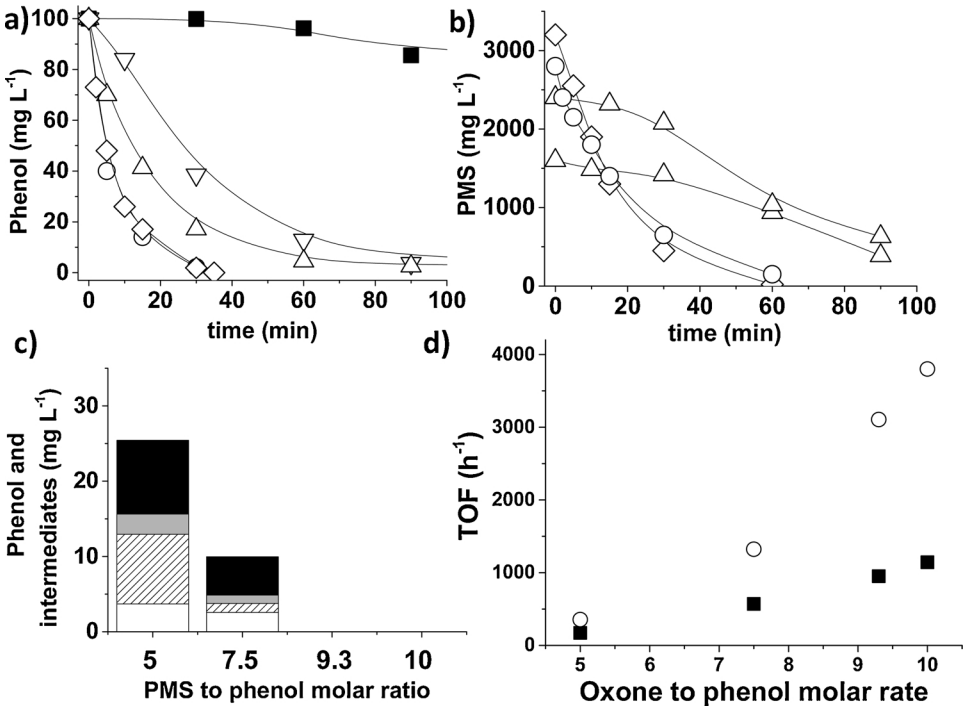

Fig. 10. Phenol degradation (a), PMS decomposition (b), remaining phenol and intermediates (c) and TOF for phenol degradation (○) and PMS decomposition (■) measured at 15 min (d) using Co_{ox}/ACN with different PMS dosages: 1600 mg L^{-1} (10.5 mM, ■), 2400 mg L^{-1} (7.9 mM, ○), 2800 mg L^{-1} (9.1 mM, ▲), 3200 mg L^{-1} (10.5 mM, □) and 4000 mg L^{-1} (13.5 mM, ●). Reaction Conditions: Catalyst (200 mg L^{-1}; 0.0067 mM of supported cobalt), phenol (100 mg L^{-1}), PMS (as indicated), 20 °C, initial pH 7.

H_2O_2 and Co_{ox}(0.2 wt%)/ACN as catalyst does not take place at neither pH value of 4 or 7. This observation agrees with previous reports showing the higher activity of the homogeneous Co^{2+}/PMS systems respect to Co^{2+}/H_2O_2 [52,53].

The influence of the temperature on the catalytic activity for PMS activation and phenol degradation using Co_{ox}/ACN as catalyst allowed an estimation of the apparent activation energy for these processes at pH 7 (Fig. 11). The estimated Ea for PMS decomposition and phenol degradation is about 30 and 32 kJ mol^{-1}, respectively. These Ea values indicate that the catalytic ROS generated during the PMS decomposition, such as $SO_4^{\cdot -}$ and $HO^{\cdot}$ (see reaction mechanism below), react in an almost barrierless process for phenol degradation. Furthermore, the lower Ea values at pH 7 compared to pH 4 reinforces the idea that is possible to develop AOP based on cobalt-catalyzed PMS activation for aqueous pollutant degradation at neutral pH values. These low Ea values obtained with Co_{ox}(0.2 wt%)/ACN compare favorably with similar systems based on cobalt oxide doped carbon aerogel (Ea for phenol 62.9 kJ mol^{-1}, pH not indicated) [21], cobalt oxide loaded on carbon xerogel (Ea for phenol degradation 48.3 kJ mol^{-1}, pH not indicated) [50], cobalt oxide on activated carbon (Ea for phenol degradation 59.7 kJ mol^{-1}, pH not indicated) [20], and other cobalt catalysts on other supports on such as ZSM5, mesoporous silicas such as SBA-15 [54] or SiO_2[37] with values ranging between 61.7 and 75.5 kJ mol^{-1}. While the previous commented literature Ea values refer to phenol degradation analogous Ea data referring to PMS decomposition are not available. It should be, however, commented the Ea for PMS decomposition is also an important kinetic parameter when comparing two activities of different catalysts, since it refers to the generation of the primary reactive oxygen radicals.

The stability of the Co_{ox}/ACN catalyst was assessed by performing eight consecutive uses of the same sample at pH 7 without observing decrease of the catalytic activity (Fig. 12a,b). Cobalt leaching from the solid catalyst to the solution after running the reaction at pH 7 was below detection limit (< 1.0 µg/L). The absence of cobalt leaching from Co_{ox}(0.2 wt%)/ACN catalyst compares favorably with the cobalt leaching measured for PMS activation when using SiO_2, TiO_2 or Al_2O_3 as support with values of cobalt leaching of 0.75, 2.83 or 0.94 mg L^{-1}, respectively (pH not indicated) [45]. Other systems based on cobalt oxide on carbon aerogel resulted in cobalt leaching around 1 mg L^{-1} (pH of reaction not indicated) and concomitant decrease of catalytic activity for phenol degradation upon reuse [21]. In other study, Co NPs embedded on carbon nanofibers resulted in a quite stable catalyst for PMS activation, although still a cobalt leaching of 20 µg L^{-1} was measured [47]. Another study that employed cobalt supported on TiO_2 as photocatalyst under UV irradiation have resulted in cobalt leaching values of 25 µg L^{-1} [18]. In our case, blank control experiments using this trace amount of cobalt to promote phenol degradation by PMS at pH 7 or 4 resulted in negligible catalytic activity indicating the heterogeneity of the reaction process. Importantly, TEM images of eight-times used Co_{ox}(0.2 wt%)/ACN shows that metal NP aggregation does

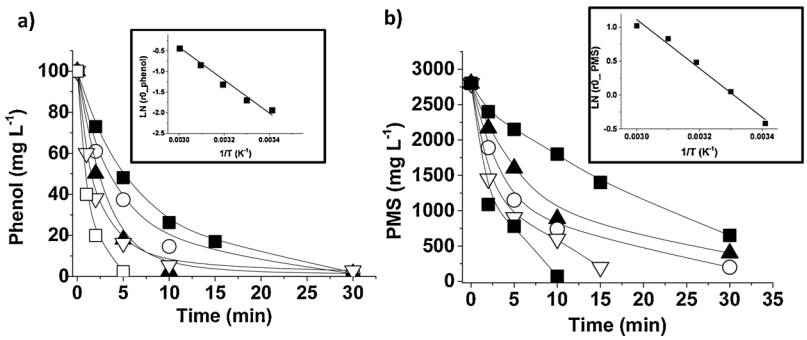

Fig. 11. Phenol degradation (a) and PMS decomposition (b) using Co_{ox}/ACN at 20 °C (■), 30 °C (○), 40 °C (▲) and 50 °C (▽). The inset shows the estimation of the apparent Ea of the process. Reaction conditions: Catalyst (200 mg L^{-1}; 0.0067 mM of supported cobalt), phenol (100 mg/L; 1.06 mM), PMS (2800 mg L^{-1}; 9.1 mM), temperature as indicated, initial pH 7.

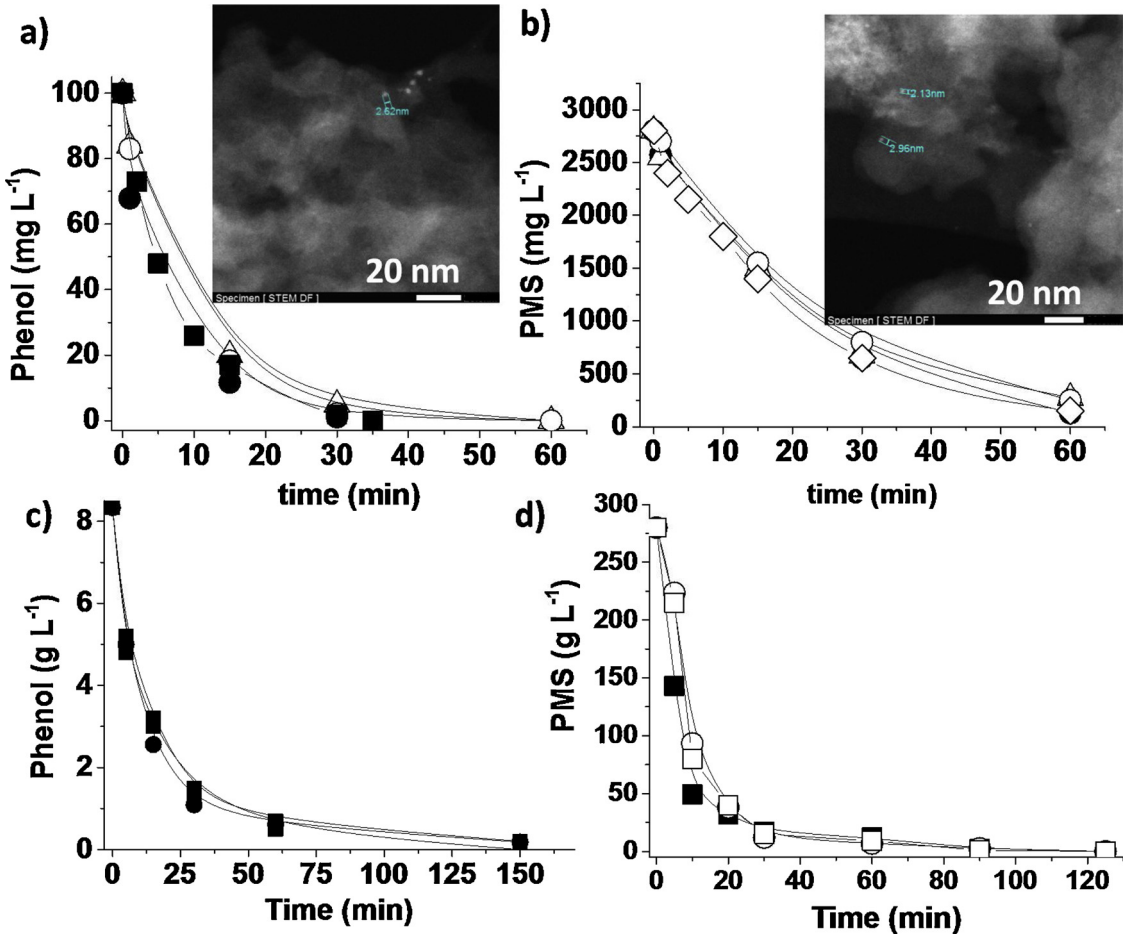

Fig. 12. Reusability of Co_{ox}/ACN at pH 7 and 20 °C under regular (a, b) or under productivity test (c, d) conditions for phenol degradation (a, c) and PMS decomposition (b, c). Legend: first cycle (■), third cycle (●), fifth cycle (Δ) and eighth cycle (○). Regular reaction conditions: Catalyst (200 mg L^{-1}; 0.0067 mM of supported cobalt), phenol (100 mg L^{-1}; 1.06 mM), PMS (2800 mg L^{-1}, 9.1 mM), 20 °C, pH 7. Productivity reaction conditions: Catalyst (200 mg L^{-1}; 0.0067 mM of supported cobalt), phenol (10 g/L; 106.4 mM), PMS (280 g L^{-1}, 912 mM), 20 °C, initial pH 7.

not occur (Fig. 12a and b inset).

Furthermore, productivity experiments using a high concentration of phenol (10 g L^{-1}; 106.4 mM) and PMS (280 g L^{-1}; 912 mM) respect to the catalyst (200 mg L^{-1}; 0.0067 mM of supported cobalt) allow determining an accumulated turnover number (TON) after three cycles for phenol and PMS decomposition as high as ~39,000 and ~400,000, respectively (Fig. 12c,d). Similarly, TOF values for the first catalytic cycle about 68,000 and $8{\cdot}10^5$ h^{-1} for phenol degradation and PMS, respectively, were estimated at 5 min of reaction. These TON and TOF values are much higher compared to those reported in the literature using heterogeneous metal catalysts for water pollutant degradation using PMS as oxidant that frequently are lower than 100 [9,20,21,45,47,50,51,55–57]. As commented, different heterogeneous catalysts have been reported for PMS activation but, however, most of these papers do not measure PMS decomposition and, therefore, estimation of TOF and TON values for PMS decomposition is not possible in those cases.

In this study, the good stability of the Co_{ox}/ACN catalyst may be attributed to the presence of oxygen functional groups able to establish strong anchoring interaction with the cobalt NPs. The reusability data of Co_{ox}/ACN compares favorably with analogous catalyst based on oxidized cobalt NPs supported on carbon microspheres [57], on SiO_2 [17,45] or on TiO_2 [45] and Al_2O_3 [45], among others [58], that suffer deactivation upon reuse.

3.4. Reaction mechanism

In order to determine the reactive oxygen species generated in the catalytic system for PMS activation by the action of Co_{ox}/ACN as catalyst, a series of selective radical quenching experiments and EPR measurements were performed. As preliminary experiments the influence of ambient oxygen in the catalytic reaction was evaluated. The presence of oxygen only slightly accelerates in comparison with inert atmosphere (Fig. S18) both phenol degradation and PMS decomposition, therefore, suggesting that oxygen participates in the radical reaction mechanism. The possible formation of radical species was further evaluated using DMSO, methanol and *tert*-butanol as radical scavengers [19,59,60]. The inhibition of the reaction by presence of DMSO and methanol indicate that hydroxyl and sulfate radicals are involved in phenol degradation [59–61]. *tert*-Butanol quenching has been considered as a specific agent of hydroxyl radicals [59,60]. Accordingly, the difference in the temporal profile of phenol degradation in the absence or presence of *tert*-butanol can also serve to indirectly evaluate the contribution of sulfate radicals. As it can be seen in Fig. 13, the presence of a large excess of *tert*-butanol quenches partially phenol degradation indicating that both $SO_4^{\cdot -}$ and $HO^{\cdot}$ radicals are simultaneously involved. On one hand, *tert*-butanol decreases the initial reaction rate of phenol degradation by about 60% (attributed to the contribution of hydroxyl radicals to phenol degradation in the absence of *tert*-butanol), but on the other hand phenol is still degraded in 100% at longer reaction times (degradation caused by contribution due to unquenchable sulfate radicals).

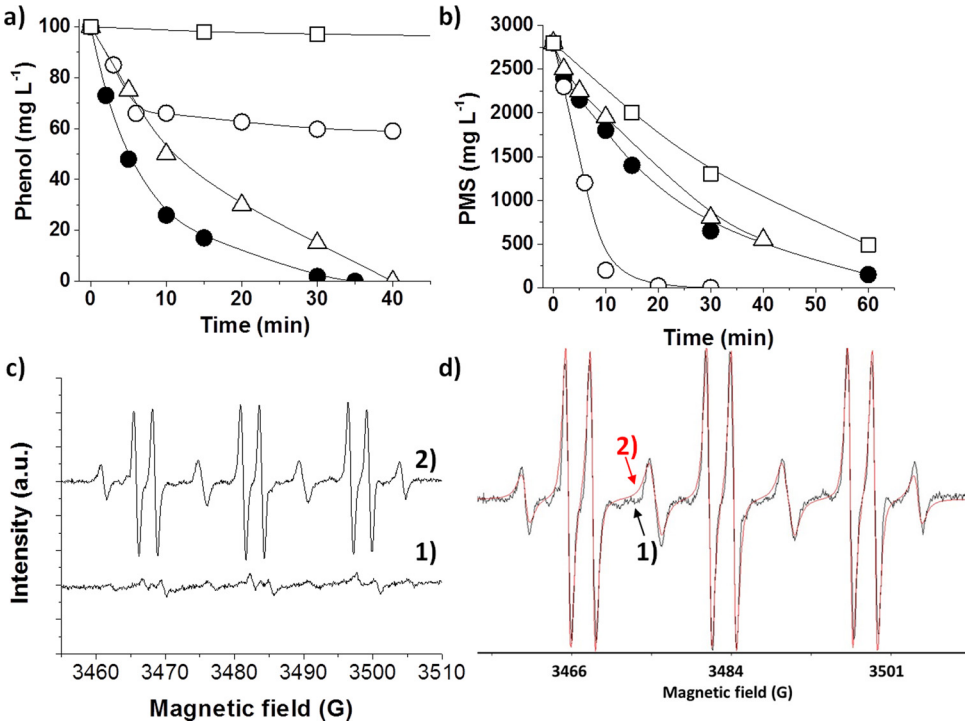

Fig. 13. (a) Phenol degradation and (b) PMS decomposition using Co_{ox}/ACN as catalyst. Legend: air atmosphere (●), air atmosphere with the presence of DMSO (□), methanol (○) or *tert*-butanol (Δ) as radical quenchers. Reaction conditions: Catalyst (200 mg L^{-1}; 0.0067 mM of supported cobalt), phenol (100 mg L^{-1}; 1.06 mM), PMS (2800 mg L^{-1}, 9.1 mM), 20 °C, initial pH 7, radical quencher to PMS molar ratio 10. (c) Experimental EPR spectra recorded in H2O at pH 7 in the presence of PMS and the absence (1) or in the presence of Coox/ACN catalyst (2) after 15 min reaction time. (d) Experimental (1, black line) and simulated (2, red line) EPR spectra under (c) conditions. Hyperfine coupling constants of PBN-OH (~85% area) AG_N = 15.4 and AG_H = 2.7 and *tert*-butyl aminoxyl from degraded PBN AG_N = 15.58 and AG_H = 13.90 (For interpretation of the references to colour in this figure legend, the reader is referred to the web version of this article.).

Additional mechanistic studies were performed by using PBN as trapping agent followed by EPR. PBN has been reported to trap both $SO_4^{\cdot -}$ and $HO^{\cdot}$ radicals [62]. EPR measurements using PBN as spin trap clearly shows the formation of the PBN−OH adduct under conditions relevant to phenol degradation. Note that the control in the absence of Co_{ox}/ACN only allows to detect very weak EPR signals, indicating that $^{\cdot}OH$ radicals are formed mainly due to the activity of the Co_{ox}/ACN catalyst (Fig. 13c and d).

Based on these results a one-electron transfer process from Co(II) species to PMS leading to the generation of sulfate radicals is proposed (Eq. (9)). Then, catalytic cycle involves reduction of Co(III) to Co(II) with formation of $SO_5^{\cdot -}$ radicals (Eq. (10)) [10,11]. $SO_4^{\cdot -}$ radicals can also be generated by reaction of $SO_5^{\cdot -}$ under acid conditions (Eq. (11)) [10,11]. In addition, $SO_4^{\cdot -}$ radicals can be converted into $HO^{\cdot}$ radicals according Eq. (12) [10].

$$\text{Cat-Co}^{2+}\text{-sites} + HSO_5^- \rightarrow \text{Cat-Co}^{3+}\text{-sites} + SO_4^{\cdot -} + HO^- \quad (9)$$

$$\text{Cat-Co}^{3+}\text{-sites} + HSO_5^- \rightarrow \text{Cat-Co}^{2+}\text{-sites} + SO_5^{\cdot -} + H^+ \quad (10)$$

$$\text{Cat} - \text{Co}^{2+}\text{-sites} + SO_5^{\cdot -} + H^+ \rightarrow \text{Cat-Co}^{3+}\text{-sites} + SO_4^{\cdot -} + HO^- \quad (11)$$

$$SO_4^{\cdot -} + H_2O \rightarrow HSO_4^- + HO^{\cdot} \quad (12)$$

4. Conclusions

The present manuscript has shown the different catalytic behavior of a series of cobalt-containing ACs as a function of the surface pretreatment and metal oxidation state. It has been found that the catalyst activity for AOP using PMS at pH 7 correlates well with the cobalt particle size, the smaller the dimension, the higher the catalyst activity. Furthermore, the oxidized supported cobalt NPs are catalytically more active than the reduced ones. In this regard, it has been established in the present study that by introducing oxygenated functional groups in AC by a chemical treatment using nitric acid (ACN), it is possible to obtain the cobalt oxide NPs with small average particle size (4.7 ± 0.05 nm) and, therefore, exhibiting an enhanced catalytic activity towards PMS decomposition and phenol degradation. Furthermore, these surface oxygenated groups and the strong anchoring of oxidized cobalt NPs are also responsible for the stability of these NPs, minimizing their growth and allowing their reusability up to eight cycles without decay and the absence of cobalt leaching. It is remarkable that no cobalt leaching is detectable. Productivity tests using a large excess of phenol and PMS respect to the Co_{ox}(0.2 wt%)/ACN catalyst allow to determine TON/TOF values as high as 39,000/68,000 h^{-1} for phenol and 400,000/8·10^5 h^{-1} for PMS at pH 7 and 20 °C, respectively. In this way the Co_{ox}(0.2 wt%)/ACN catalyst compares favorably with those previously reported in the literature is herein described.

Acknowledgements

Financial support by the Spanish Ministry of Economy and Competitiveness (Severo Ochoa, CTQ2015-65963-CQ-R1) and CTQ2014-53292-R is gratefully acknowledged. Generalitat Valenciana is also thanked for funding (Prometeo 2017/083). S.N. thanks financial support by the Fundación Ramón Areces (XVIII Concurso Nacional para la Adjudicación de Ayudas a la Investigación en Ciencias de la Vida y de la Materia, 2016).

Appendix A. Supplementary data

Supplementary material related to this article can be found, in the online version, at doi:https://doi.org/10.1016/j.apcatb.2019.02.043.

References

[1] K. Ayoub, E.D. van Hullebusch, M. Cassir, A. Bermond, Application of advanced oxidation processes for TNT removal: a review, J. Hazard. Mater. 178 (2010) 10–28.
[2] M. Cheng, G. Zeng, D. Huang, C. Lai, P. Xu, C. Zhang, Y. Liu, Hydroxyl radicals based advanced oxidation processes (AOPs) for remediation of soils contaminated with organic compounds: a review, Chem. Eng. J. 298 (2016) 582–598.
[3] E. Neyens, J. Baeyens, A review of classic Fenton's peroxidation as an advanced oxidation technique, J. Hazard. Mater. 98 (2003) 33–50.
[4] M. Pera-Titus, V. García-Molina, M.A. Baños, J. Giménez, S. Esplugas, Degradation of chlorophenols by means of advanced oxidation processes: a general review, Appl. Catal. B: Environ. 47 (2004) 219–256.
[5] J.J. Pignatello, E. Oliveros, A. MacKay, Advanced oxidation processes for organic contaminant destruction based on the fenton reaction and related chemistry, Crit. Rev. Environ. Sci. Technol. 36 (2006) 1–84.

[6] K. Demeestere, J. Dewulf, H. Van Langenhove, Heterogeneous photocatalysis as an advanced oxidation process for the abatement of chlorinated, monocyclic aromatic and sulfurous volatile organic compounds in air: state of the art, Crit. Rev. Environ. Sci. Technol. 37 (2007) 489–538.
[7] S. Malato, P. Fernández-Ibáñez, M.I. Maldonado, J. Blanco, W. Gernjak, Decontamination and disinfection of water by solar photocatalysis: recent overview and trends, Cat. Today 147 (2009) 1–59.
[8] I. Oller, S. Malato, J.A. Sánchez-Pérez, Combination of advanced oxidation processes and biological treatments for wastewater decontamination—a review, Sci. Total Environ. 409 (2011) 4141–4166.
[9] G.P. Anipsitakis, E. Stathatos, D.D. Dionysiou, Heterogeneous activation of oxone using Co3O4, J. Phys. Chem. B 109 (2005) 13052–13055.
[10] P. Hu, M. Long, Cobalt-catalyzed sulfate radical-based advanced oxidation: a review on heterogeneous catalysts and applications, Appl. Catal. B. Environ. 181 (2016) 103–117.
[11] F. Ghanbari, M. Moradi, Application of peroxymonosulfate and its activation methods for degradation of environmental organic pollutants: review, Chem. Eng. J. 310 (2017) 41–62.
[12] D.L. Ball, J.O. Edwards, The kinetics and mechanism of the decomposition of Caro's acid, J. Am. Chem. Soc. 78 (1956) 1125–1129.
[13] Council Directive 98/83/EC of 3 November 1998 on the quality of water intended for human consumption.
[14] S. Navalon, M. Alvaro, H. Garcia, Heterogeneous Fenton catalysts based on clays, silicas and zeolites, Appl. Catal. B: Environ. 99 (2010) 1–26.
[15] S. Navalon, A. Dhakshinamoorthy, M. Alvaro, H. Garcia, Heterogeneous Fenton catalysts based on activated carbon and related materials, ChemSusChem 4 (2011) 1712–1730.
[16] E.G. Garrido-Ramírez, B.K.G. Theng, M.L. Mora, Clays and oxide minerals as catalysts and nanocatalysts in Fenton-like reactions—a review, Appl. Clay Sci. 47 (2010) 182–192.
[17] P. Shukla, H. Sun, S. Wang, H.M. Ang, M.O. Tadé, Nanosized Co3O4/SiO2 for heterogeneous oxidation of phenolic contaminants in waste water, Separ. Purif. Technol. 77 (2011) 230–236.
[18] Q. Yang, H. Choi, Y. Chen, D.D. Dionysiou, Heterogeneous activation of peroxymonosulfate by supported cobalt catalysts for the degradation of 2,4-dichlorophenol in water: the effect of support, cobalt precursor, and UV radiation, Appl. Catal. B. Environ. 77 (2008) 300–307.
[19] Q.J. Yang, H. Choi, D.D. Dionysiou, Nanocrystalline cobalt oxide immobilized on titanium dioxide nanoparticles for the heterogeneous activation of peroxymonosulfate, Appl. Catal. B: Environ. 74 (2007) 170–178.
[20] P.R. Shukla, S. Wang, H. Sun, H.M. Ang, M. Tadé, Activated carbon supported cobalt catalysts for advanced oxidation of organic contaminants in aqueous solution, Appl. Catal. B: Environ. 100 (2010) 529–534.
[21] Y. Hardjono, H. Sun, H. Tian, C.E. Buckley, S. Wang, Synthesis of Co oxide doped carbon aerogel catalyst and catalytic performance in heterogeneous oxidation of phenol in water, Chem. Eng. J. 174 (2011) 376–382.
[22] P.R. Shukla, S.B. Wang, K. Singh, H.M. Ang, M.O. Tade, Cobalt exchanged zeolites for heterogeneous catalytic oxidation of phenol in the presence of peroxymonosulphate, Appl. Catal. B: Environ. 99 (2010) 163–169.
[23] K.-Y. Andrew Lin, H.-A. Chang, Zeolitic imidazole framework-67 (ZIF-67) as a heterogeneous catalyst to activate peroxymonosulfate for degradation of Rhodamine B in water, J. Taiwan Inst. Chem. Eng. 53 (2015) 40–45.
[24] Q. Yang, H. Choi, S.R. Al-Abed, D.D. Dionysiou, Iron-cobalt mixed oxide nanocatalysts: heterogeneous peroxymonosulfate activation, cobalt leaching, and ferromagnetic properties for environmental applications, Appl. Catal. B: Environ. 88 (2009) 462–469.
[25] X. Duan, Z. Ao, H. Zhang, M. Saunders, H. Sun, Z. Shao, S. Wang, Nanodiamonds in sp2/sp3 configuration for radical to nonradical oxidation: core-shell layer dependence, Appl. Catal. B: Environ. 222 (2018) 176–181.
[26] X. Duan, H. Sun, S. Wang, Metal-free carbocatalysis in advanced oxidation reactions, Acc. Chem. Res. 51 (2018) 678–687.
[27] A. Dhakshinamoorthy, S. Navalon, M. Alvaro, H. Garcia, Metal nanoparticles as heterogeneous Fenton catalyst, ChemSusChem 5 (2012) 46–64.
[28] K. Takahashi, S. Yokoyama, T. Matsumoto, J.L.C. Huaman, H. Kaneko, J.-Y. Piquemal, H. Miyamura, J. Balachandran, Towards a designed synthesis of metallic nanoparticles in polyols-elucidation of the redox scheme in a cobalt-ethylene glycol system, New J. Chem. 40 (2016) 8632–8642.
[29] C. López-Santos, F. Yubero, J. Cotrino, A.R. González-Elipe, Lateral and in-depth distribution of functional groups on diamond-like carbon after oxygen plasma treatments, Diam. Relat. Mater. 20 (2011) 49–56.
[30] D. Sempere, S. Navalon, M. Dančíková, M. Alvaro, H. Garcia, Influence of pretreatments on commercial diamond nanoparticles on the photocatalytic activity of supported gold nanoparticles under natural Sunlight irradiation, Appl. Catal. B: Environ. 142–143 (2013) 259–267.
[31] R. Martín, S. Navalon, M. Alvaro, H. Garcia, Optimized water treatment by combining catalytic Fenton reaction using diamond supported gold and biological degradation, Appl. Catal. B: Environ. 103 (2011) 246–252.
[32] S. Wacławek, K. Grübel, M. Cerník, Simple spectrophotometric determination of monopersulfate, Spectrochim. Acta A. 149 (2015) 928–933.
[33] L. Fan, C. Moreno-Castilla, M.A. Ferro-Garcia, J.P. Joly, I. Bautista-Toledo, F. Carrasco-Marin, J. Rivera-Utrilla, Surface modifications by nitric acid, hydrogen peroxide, and ammonium peroxydisulfate treatments activated carbon, Langmuir 11 (1995) 4386–4392.
[34] M.S. Shafeeyan, W.M.A.W. Daud, A. Houshmand, Ahmad Shamiri, A review on surface modification of activated carbon for carbon dioxide adsorption, J. Anal. Appl. Pyrol. 89 (2010) 143–151.
[35] N. Shimodaira, A. Masui, Raman spectroscopic investigations of activated carbon materials, J. Appl. Phys. 92 (2002) 902–909.
[36] J.-H. Zhou, Z.-J. Sui, J. Zhu, P. Li, D. Chen, Y.-C. Dai, W.-K. Yuan, Characterization of surface oxygen complexes on carbon nanofibers by TPD, XPS and FT-IR, Carbon 45 (2007) 785–796.
[37] B.S. Girgis, Y.M. Temerk, M.M. Gadelrab, I.D. Abdullah, X-ray diffraction patterns of activated carbons prepared under various conditions, Carbon Sci. 2 (2007) 95–100.
[38] J.C. Espinosa, S. Navalón, M. Álvaro, H. García, Copper nanoparticles supported on diamond nanoparticles as a cost-effective and efficient catalyst for natural sunlight assisted Fenton reaction, Catal. Sci. Technol. 6 (2016) 7077–7085.
[39] R. Shi, G. Chen, W. Ma, D. Zhang, G. Qiu, X. Liu, Shape-controlled synthesis and characterization of cobalt oxides hollow spheres and octahedra, Dalton Trans. 41 (2012) 5981–5987.
[40] J. González-Prior, R. López-Fonseca, J.I. Gutiérrez-Ortiz, B. de Rivas, Oxidation of 1,2-dichloroethane over nanocube-shaped Co3O4 catalysts, Appl. Catal. B: Environ. 199 (2016) 384–393.
[41] W. Guo, E. Yifeng, L. Gao, L. Fan, S. Yang, A catalytic nanostructured cobalt oxide electrode enables positive potential operation for the cathodic electrogenerated chemiluminescence of Ru(bpy)32+ with dramatically enhanced intensity, Chem. Commun. 46 (2010) 1290–1292.
[42] H.M. Chen, R.-S. Liu, H. Li, H.C. Zeng, Generating isotropic superparamagnetic interconnectivity for the two-dimensional organization of nanostructured building blocks, Angew. Chem. Int. Ed. 45 (2006) 2713–2717.
[43] A. Dhakshinamoorthy, S. Navalon, D. Sempere, M. Alvaro, H. Garcia, Aerobic oxidation of thiols catalyzed by copper nanoparticles supported on diamond nanoparticles, ChemCatChem 5 (2013) 241–246.
[44] I.H. Kim, H.O. Seo, E.J. Park, S.W. Han, Y.D. Kim, Low temperature CO oxidation over iron oxide nanoparticles decorating internal structures of a mesoporous alumina, Sci. Rep. 7 (2017) 40497.
[45] H. Sun, H. Liang, G. Zhou, S. Wang, Supported cobalt catalysts by one-pot aqueous combustion synthesis for catalytic phenol degradation, J. Colloid Interface Sci. 394 (2013) 394–400.
[46] S. Navalon, A. Dhakshinamoorthy, M. Alvaro, H. Garcia, Metal nanoparticles supported on two-dimensional graphenes as heterogeneous catalysts, Coord. Chem. Rev. 312 (2016) 99–148.
[47] K.A. Lin, W.C. Tong, Y. Du, Cobalt-embedded carbon nanofiber derived from a coordination polymer as a highly efficient heterogeneous catalyst for activating oxone in water, Chemosphere 195 (2018) 272–281.
[48] J. Sun, X. Li, J. Feng, X. Tian, Oxone/Co2+ oxidation as an advanced oxidation process: comparison with traditional Fenton oxidation for treatment of landfill leachate, Water Res. 43 (2009) 4363–4369.
[49] W. Guo, S. Su, C. Yi, Z. Ma, Degradation of antibiotics amoxicillin by Co3O4-catalyzed peroxymonosulfate system, Environ. Prog. Sustain. Energy 32 (2013) 193–197.
[50] H. Sun, H. Tian, Y. Hardjono, C.E. Buckley, S. Wang, Preparation of cobalt/carbon-xerogel for heterogeneous oxidation of phenol, Catal. Today 186 (2012) 63–68.
[51] Y. Wang, H. Sun, H.M. Ang, M.O. Tadé, S. Wang, Facile synthesis of hierarchically structured magnetic MnO2/ZnFe2O4 hybrid materials and their performance in heterogeneous activation of peroxymonosulfate, ACS Appl. Mater. Interfaces 6 (2014) 19914–19923.
[52] G.P. Anipsitakis, D.D. Dionysiou, Radical generation by the interaction of transition metals with common oxidants, Environ. Sci. Technol. 38 (2004) 3705–3712.
[53] S.K. Ling, S. Wang, Y. Peng, Oxidative degradation of dyes in water using Co2+/H2O2 and Co2+/peroxymonosulfate, J. Hazard. Mater. 178 (2010) 385–389.
[54] P. Shukla, H. Sun, S. Wang, H.M. Ang, M.O. Tadé, Co-SBA-15 for heterogeneous oxidation of phenol with sulfate radical for wastewater treatment, Catal. Today 175 (2011) 380–385.
[55] Y. Wang, H. Sun, H.M. Ang, M.O.O. Tadé, S. Wang, 3D-hierarchically structured MnO2 for catalytic oxidation of phenolsolutions by activation of peroxymonosulfate: structure dependenceand mechanism, Appl. Catal. B. Environ. 164 (2015) 159–167.
[56] S.B. Hammoudaa, F. Zhaoa, Z. Safaeia, V. Srivastavaa, D.L. Ramasamya, S.I. Iftekhara, S. kalliola, M. Sillanpää, Degradation and mineralization of phenol in aqueous medium by heterogeneous monopersulfate activation on nanostructured cobalt based-perovskite catalysts ACoO3 (A = La, Ba, Sr and Ce): characterization, kinetics and mechanism study, Appl. Catal. B. Environ. 215 (2017) 60–73.
[57] G. Zhou, L. Zhou, H. Sun, H.M. Ming Ang, M.O. Tadé, S. Wang, Carbon microspheres supported cobalt catalysts forphenol oxidation with peroxymonosulfate, Chem. Eng. Res. Des. 101 (2015) 15–21.
[58] S. Muhammad, E. Saputra, H. Sun, H.-M. Ang, M.O.O. Tadé, S. Wang, Heterogeneous catalytic oxidation of aqueous phenol on red mud-supported cobalt catalysts, Ind. Eng. Chem. Res. 51 (2012) 15351–15359.
[59] X. Cheng, H. Guo, Y. Zhang, X. Wu, Y. Liu, Non-photochemical production of singlet oxygen via activation of persulfate by carbon nanotubes, Water Res. 113 (2017) 80–88.
[60] X. Pan, J. Chen, N. Wu, Y. Qi, X. Xu, J. Ge, X. Wang, C. Li, R. Qu, V.K. Sharma, Z. Wang, Degradation of aqueous 2,4,4′-trihydroxybenzophenone by persulfate activated with nitrogen doped carbonaceous materials and the formation of dimer products, Water Res. 143 (2018) 176–187.
[61] A. Rastogi, S.R. Al-Abed, D.D. Dionysiou, Sulfate radical-based ferrouseperoxymonosulfate oxidative system for PCBs degradation in aqueous and sediment systems, Appl. Catal. B 85 (2009) 171–179.
[62] M.J. Burkitt, R.P. Mason, Direct evidence for in vivo hydroxyl-radical generation in experimental iron overload: an ESR spin-trapping investigation, Proc. Natl. Acad. Sci. U. S. A. 88 (1991) 8440–8444.